Modelling the coefficient of thermal expansion in Ni-based superalloys and bond coatings

KARUNARATNE, M. S. A., KYAW, Si <http://orcid.org/0000-0001-8568-500X>, JONES, A., MORRELL, R. and THOMSON, R. C.

Published version

KARUNARATNE, M. S. A., KYAW, Si, JONES, A., MORRELL, R. and THOMSON, R. C. (2016). Modelling the coefficient of thermal expansion in Ni-based superalloys and bond coatings. Journal of Materials Science, 51 (9), 4213-4226.

J Mater Sci (2016) 51:4213–4226
DOI 10.1007/s10853-015-9554-3

Modelling the coefficient of thermal expansion in Ni-based superalloys and bond coatings

M. S. A. Karunaratne[1] · S. Kyaw[2] · A. Jones[2] · R. Morrell[3] · R. C. Thomson[1]

Received: 12 August 2015 / Accepted: 30 October 2015 / Published online: 8 February 2016

Abstract The coefficient of thermal expansion (CTE) of nickel-based superalloys and bond coat layers was modelled by considering contributions from their constituent phases. The equilibrium phase composition of the examined materials was determined using thermodynamic equilibrium software with an appropriate database for Ni-based alloys, whereas the CTE and elastic properties of the principal phases were modelled using published data. The CTEs of individual phases were combined using a number of approaches to determine the CTE of the phase aggregate. As part of this work, the expansion coefficients of the superalloy IN-738LC and bond coat Amdry-995 were measured as a function of temperature and compared with the model predictions. The predicted values were also validated with the published data for the single-crystal superalloy CMSX-4 and a number of other Ni-based alloy compositions at 1000 K. A very good agreement between experiment and model output was found, especially up to 800 °C. The modelling approaches discussed in this paper have the potential to be an extremely useful tool for the industry and for the designers of new coating systems.

✉ M. S. A. Karunaratne
M.Karunaratne@lboro.ac.uk

S. Kyaw
Si.Kyaw@nottingham.ac.uk

A. Jones
Arthur.Jones@nottingham.ac.uk

R. Morrell
Roger.Morrell@npl.co.uk

R. C. Thomson
R.C.Thomson@lboro.ac.uk

[1] Department of Materials, Loughborough University, Ashby Road, Loughborough LE11 3TU, UK

[2] Department of Mechanical, Materials and Manufacturing Engineering, University of Nottingham, University Park, Nottingham NG7 2RD, UK

[3] National Physical Laboratory, Hampton Road, Teddington, Middlesex TW11 0LW, UK

Introduction

Background

Gas turbine components used in aero- and land-based engines are designed to operate at high temperatures and pressures in corrosive environments. These days, such conditions are satisfied by coated nickel-based superalloys [1, 2]. Over the years, Ni-based superalloy compositions have evolved such that they are complex alloys for the most demanding of applications containing more than ten elements, and often cast in single-crystal form. Superalloys derive their strength and creep resistance from a precipitation-hardened microstructure comprising an ordered Ni_3Al-based precipitate phase (γ') in a solution-hardened fcc Ni (γ) matrix (e.g. [3]). The mechanical properties of a modern superalloy are optimised for high-temperature creep and fatigue properties over corrosion protection, and hence, there is an increasing emphasis on coating systems for environmental and thermal protection. A typical coating system for a turbine blade for the high pressure section of a gas turbine consists of a ceramic thermal barrier top coat (TBC) and an intermediate metallic bond coat (BC) between the TBC and substrate. The ceramic TBC is normally made from yttria-stabilised zirconia (YSZ), and the overlay BC is of the MCrAlY type but, more generally, its composition can be represented by the MCrAlX type where M mainly refers to Ni and / or Co, and sometimes heavy

elements such as Ta. A reactive element is represented by X, such as Y, Hf and/or Si.

The role of the BC is to provide a sacrificial oxidation barrier for the substrate, whilst also acting as a binding interface for the TBC (e.g. [4]). During service, the BC develops a surface layer of thermally grown oxide (TGO), which consists primarily of α-Al_2O_3. The TGO protects against further oxidation of the BC by the combustion gases which are believed to permeate the porous TBC freely. The BC contains a relatively high amount of Al and Cr to maintain a TGO layer which has to withstand many cycles of breakage (spallation) and regrowth. The high Al concentration in the BC gives rise to the NiAl (β) phase, which is commonly present with the γ, and sometimes with γ', phases. Some BC compositions which have a large amount of Cr also contain the bcc α-Cr phase in significant amounts.

In the service environment, the Al and Cr concentrations of the BC decrease as a result of interdiffusion with the substrate and also due to consumption by the scale formation process. This results in the initial BC, which generally has a high fraction of β, transforming into a microstructure consisting of γ' and γ phases. Furthermore, as Al is removed from the BC surface by scale formation, an outer layer depleted of β is created, the extent of which is often an indicator of the remaining life of the BC. At the same time, the heavy elements present in the substrate migrate into the BC, giving rise to an interdiffusion zone (IDZ) near the BC/substrate interface. The IDZ is generally rich in γ' and is often populated by the topologically close-packed (TCP) phases, which are considered harmful for their potential for weakening the matrix by removing solution hardening elements.

The complexity of the layered coating system can give rise to in and out of plane thermal stresses. Due to the variations in their chemistry and atomic bonding, the TBC, TGO, BC and substrate have considerably different thermal expansion characteristics. These CTE differentials can cause substantial mechanical stresses between the layers during production and service, which with additional stresses created due to the growth of the TGO, can cause de-lamination and/or cracking. Furthermore, the expansion properties of the layers gradually change over time with the evolving microstructure. Fortunately, the thermal stresses created can relax at high temperature by processes such as creep [5]. On the other hand, the structure is more vulnerable to mechanical failure during cooling due to the lack of flow processes at low temperatures and also because of the increase in brittle phases such as β in the BC. The TGO is particularly susceptible to failure, and stresses caused by thermal expansion difference are acknowledged to be the general cause for TGO spallation. Thermal stresses also set upper limits for the thickness of layers of TBC and TGO.

Therefore, it is necessary to minimise thermally induced stresses by reducing the thermal expansion mismatch between layer interfaces when designing coating systems. The BC compositions in particular can be tailored to reduce such stresses. Although the influence of phase constitution on the CTE of substrates and bond coat has been acknowledged (e.g. [6]), most traditional models are mainly empirical in nature and do not explicitly take the phase composition into account. However, there are now thermodynamic modelling tools available which can, along with a properly assessed thermodynamic parameter database, predict the equilibrium phase structure of bond coat compositions and substrates. In the modelling work described here, thermodynamic computation tools have been used to generate a more accurate prediction of the CTE of a material by accounting for individual phase volumes and their CTE characteristics at different temperatures.

Coefficient of thermal expansion (CTE)

Most materials expand when heated and shrink when cooled. The associated change in length with temperature is measured using the coefficient of linear thermal expansion $\bar{\alpha}$ which is defined by

$$\bar{\alpha} = \frac{l - l_0}{l_0(T - T_0)}, \tag{1}$$

where l is the expanded length of a specimen at temperature T and l_0 is the initial length at temperature T_0, which is generally taken to be room ambient 20 °C (293 K). The CTE is also defined as the fractional increase in length per unit temperature increment as follows:

$$\alpha = \frac{1}{l}\frac{\mathrm{d}l}{\mathrm{d}T}, \tag{2}$$

where l is the length of the test piece at temperature T and α is commonly identified as expansivity or physical expansion coefficient.

The expansivity α is determined by the slope of tangent in the fractional length change versus temperature plot, whereas the mean coefficient $\bar{\alpha}$ is measured by the slope of the chord between two points on the plot. The work here is primarily concerned with $\bar{\alpha}$, which is the most technologically useful form and the focus of many studies, although some of the works referenced have reported values for α. The term CTE is used in place of $\bar{\alpha}$ throughout the article to avoid possible confusion with the α-Cr phase.

Thermal expansion coefficient of phases

Nickel-based superalloys have a phase structure consisting mainly of the γ and γ' phases. The β phase occurs in high Al-containing MCrAlY bond coatings along with the γ and sometimes, γ' phases. The α-Cr phase can also be found in

high Cr-containing MCrAlY coatings. The other phases found in the systems are TCP phases, which normally include σ, μ and P phases.

The reported CTE values of pure γ(Ni), γ'(Ni_3Al), β(NiAl) and α-Cr, which are the main phases found in a typical superalloy-MCrAlY coating system, are shown as a function of temperature in Fig. 1. The thermal expansion coefficients vary according to $CTE_{Ni} > CTE_{Ni_3Al} > CTE_{NiAl} > CTE_{\alpha-Cr}$ over the temperature range 500–1100 °C as described in more detail below.

CTE of Ni

The graph of CTE of pure Ni shown in Fig. 1 has been plotted using the equation

$$CTE_{Ni} = \left(a_0 + a_1 T^n + a_2 T^{2n} + a_3 T^{3n}\right) \times 10^{-5}, \qquad (3)$$

where the constants a_0, a_1, a_2, a_3 and n are given as -3.810, 1.633, -1.746×10^{-1}, 6.510×10^{-3} and $1/3$, respectively, which have been derived by regression in [7] using published data from a number of sources.

There have been a number of studies about the effect of common alloying elements on the CTE of Ni. Giamei et al. [8] have reported the effect of Cr, W, Re and Mo on CTE of γ-Ni at 1000 °C using Ni–10Cr, Ni–10W, Ni–8Re, Ni–20Mo and Ni–25Mo (at.%) alloys. They found that Cr has virtually no effect on expansion, whereas W, Mo and Re decreased the CTE substantially in that order on a per atom basis, and the higher Mo containing Ni–25Mo alloy has a lower CTE than the Ni–20Mo composition.

In a study conducted at lower temperatures up to 538 °C, Hull et al. [9] observed that in a 20Cr–80Ni (wt%) γ non-magnetic alloy, Mo had the most dramatic effect in reducing the α, and the effect of reduction decreases in the order of Ti, W, Si, Al, (Nb + Ta). The elements which were found to increase CTE were Mn and Fe, in that order. However, unlike the work of Giamei et al. [8] at 1000 °C, Cr was found to increase the CTE up to 23.6 wt% and then decrease.

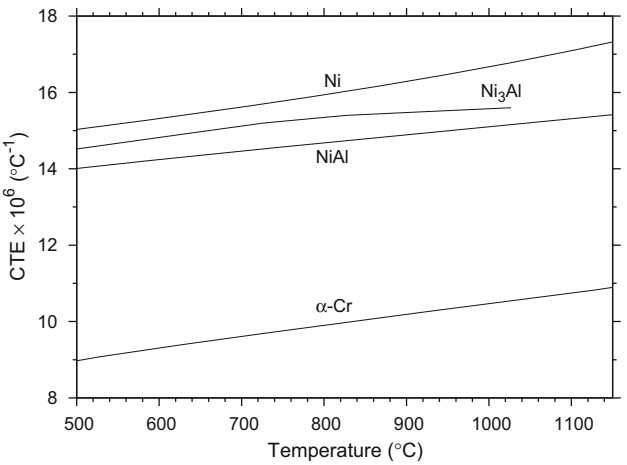

Fig. 1 The variation of CTE with temperature of pure Ni [16], Ni_3Al [16], NiAl [23] and α-Cr [24].

Morrow et al. [10] measured the effects of Mo in γ up to 1050 °C. In ternary alloys containing approximately 33 wt% Co, 35 wt% Cr, and 32 wt% Ni, they found that addition of Mo up to 6.5 wt% clearly decreased the CTE significantly, in agreement with earlier studies.

Pavlovic et al. [11] examined the CTE of fcc Ni binary alloys Ni–Cr, Ni–Mo and Ni–Re, for alloying concentrations up to 25 at.% at temperatures up to 900 K (627 °C) and reported that for all three systems, CTE decreased with increasing concentration of the second element, the addition of Cr having the least effect on CTE whereas Re the most. The findings have been compared with molecular dynamics (MD) simulation predictions carried out by Mei et al. [12], and the best agreement was found to be in the case of Mo and Re the least. A rule of mixtures equation derived by the authors shows a linear decrease of CTE with concentration for all three of these alloys, in qualitative agreement with the experimental results.

Yamamoto et al. [13] found that in Fe-free Ni alloys, Cr increased the CTE, whereas W, Mo, Al and Ti decreased it from room temperature to 700 °C. The effect of Cr and W between 20 and 800 °C was examined using a series of Ni–W, Ni–Cr, and Ni–Cr–W alloys by Dosovitskiy et al. [14]. The work revealed that W decreased the CTE considerably. The CTE could be suppressed with Cr at low temperature, but at high temperatures, Cr increased it.

Using a first-principles study, Kim et al. [15] have shown that CTE is reduced by the alloying elements Al, Cr, Hf, Pt, Y and Zr up to 1600 K (1327 °C) and that higher Pt concentrations further decreased CTE, whereas higher Al was ineffective in altering the CTE.

These studies reveal that the CTE of Ni is decreased by most common alloying elements, with the exception of Fe and Mn. The refractory elements W, Re, Mo and Ta are the most influential in reducing the CTE, but in the case of Cr, one of the most regular additions in superalloy/coating chemistries, the behaviour seems to be more complex with respect to concentration and temperature dependency.

CTE of Ni_3Al

The CTE curve of Ni_3Al up to 1300 K shown in Fig. 1 has been derived from data in [16] which are based on two sources [17, 18]. The ordered Ni_3Al phase accommodates off-stoichiometric variations within a narrow concentration band, and the influence of Al on the CTE has been investigated by several authors. Williams et al. [19] have found no significant variation in well-annealed Ni_3Al containing either 24 or 25 at.% Al. However, the measurements by Ramesh et al. [20], up to 1000 °C, have shown the CTE of

Ni–24 at.% Al to be slightly lower than that of stoichiometric Ni–25 at.% Al. However, Rao et al. [21] report that the CTE shows an increase with lower Al concentrations up to 1000 °C, and attributes the increase to a larger number of vacancies at off-stoichiometric compositions. There have been some studies on the effect of a third alloying element. Giamei et al. [8] report that CTE is reduced by the elements Mo, Ta, Nb, W and Hf up to 1000 °C. Arbuzov and Zelenkov [17] have studied the effect of Ta, Zr, V, Mn and Ti and concluded that the variation in CTE depends on the CTE of the alloying elements themselves. For example, B and Zr, which have lower values of α, decrease the CTE of Ni_3Al, whereas Hf and Ti do not alter it significantly. Porter and Maziasz [22] have measured the CTE of the commercial Ni_3Al alloy IC-221M which has the composition 15.9Al–8Cr–0.8Mo–1Zr–0.04B at.% and find the expansion of IC-221M to be very similar to published data for the commercial nickel-based superalloy Inconel 713C [16], possibly due to their similarity in composition.

CTE of NiAl

The graph of CTE of NiAl shown in Fig. 1 has been plotted using the equation

$$\begin{aligned} \mathrm{CTE}_{\mathrm{NiAl}} &= 1.16026 \times 10^{-5} + 4.08531 \times 10^{-9} T \\ &\quad -1.58368 \times 10^{-12} T^2 + 4.18374 \times 10^{-16} T^3, \end{aligned} \tag{4}$$

where T is temperature in K and is valid between 300 and 3000 K. The equation was derived by Noebe et al. [23] considering a number of published data for polycrystalline materials. It is noted that the CTE of NiAl is a strong function of temperature but not of composition. To the authors' best knowledge, there are no reported investigations on the variations of CTE with off-stoichiometric compositions in NiAl, nor on third or higher element additions.

CTE of α-Cr

The α-Cr phase, mostly found in MCrAlY coatings containing a high amount of Cr, and sometimes also in superalloys, is based on the BCC α phase of the element Cr. The graph shown in Fig. 1 is derived from data in [16] for pure Cr and is in good agreement with reported figure for α-Cr by Fritscher et al. [24] who observe that the CTE remains fairly constant at 10.0×10^{-6} °C^{-1} from room temperature up to 1000 °C.

Modelling of CTE

Appropriate modelling techniques can be divided broadly into three categories as (a) rule of mixture of elements, (b) empirical models and (c) phase-structure-based approaches.

Rule of mixture of elements

In this approach, the CTE of an alloy is composed of individual contributions of constituent elements, and in the simplest form, a simple rule of mixtures formulation can be given as

$$\bar{\alpha} = \sum \bar{\alpha}_i V_i, \tag{5}$$

where $\bar{\alpha}$ and $\bar{\alpha}_i$ are the CTEs of the alloy and constituent element i, respectively, and V_i is the atomic volume fraction of the element i.

The ability of heavy refractory elements such as Re, W, Mo, Ta and W to lower the CTE of nickel-based alloys is well documented as discussed earlier (e.g. [8, 11, 14]), and many workers have also identified these elements to have much lower CTEs themselves compared to Ni. Therefore, at least at first sight, a rule of mixtures model seems very plausible. The graphs in Fig. 2a, b illustrate this point and show how CTE varies between 500 and 1150 °C for a number of pure elements often found in the nickel-based superalloy and bond coat compositions.

Among the refractory elements, W and Mo have the lowest thermal expansion characteristics with a CTE smaller than 6×10^{-6} °C^{-1}. Figure 2b concentrates on the lower half of the graph, with elements having melting points above 2200 °C and CTE between 6.0 and 8.5 °C^{-1}.

The group of elements Cr, Ti and V, which are adjacent in the periodic table, show close expansion coefficients which vary between 9.0 and 11.0 °C^{-1}. The drop observed of CTE in the case of Ti at 882 °C is due to the phase transition from hcp (α) to bcc (β). The CTE of Co is similar to and slightly higher than that of Ni. Aluminium has the highest CTE. Since thermal expansion is related to atomic bonding, which also affects the melting point (MP), it is perhaps not surprising that W with the highest melting point 3420 °C has the lowest CTE of the group and Al with the lowest MP (660 °C) has the highest CTE.

Several authors have commented that although the presence of low expansion elements in the alloy composition reduces the CTE of an alloy, a simple rule of mixtures approach cannot be adopted universally to predict the expansion behaviour of an alloy. Pavlovic et al. [11] in their study on the effect of Cr, Re and Mo on the thermal expansion of Ni argue that the simple rule of mixtures seems to work best when the atomic volumes of the atoms in the alloy are not too different. They found that the experimental decrease in CTE with the at.% of Mo and Re is three to four times larger than the prediction of the simple rule of mixtures equation, whereas for Cr, the experimental and predicted values are quite comparable. Furthermore, the authors argue that the predicted decrease

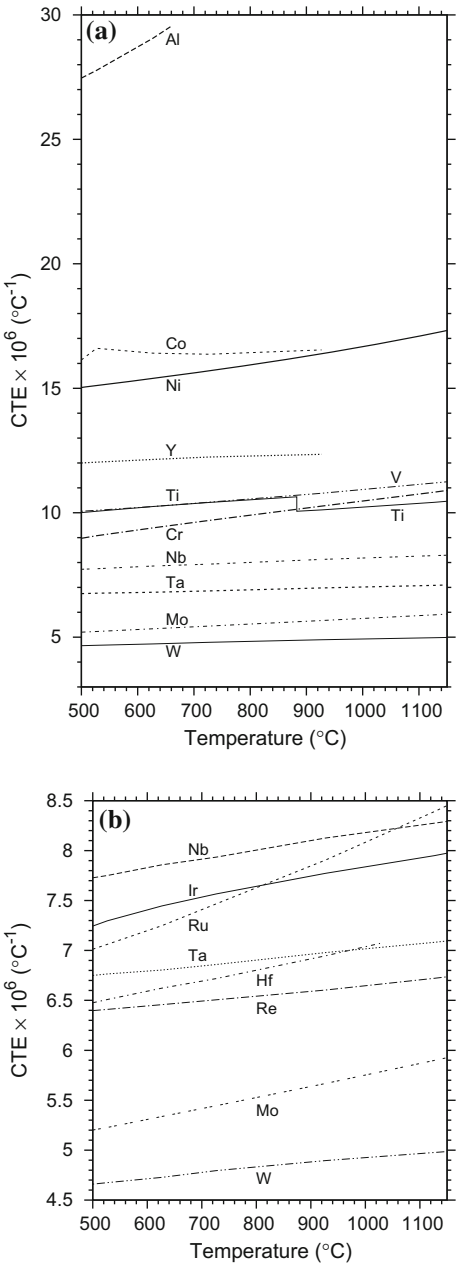

Fig. 2 The variation of CTE with temperature of a number of common elements **a** and **b**, found in nickel-based superalloys and MCrAlY bond coat compositions with **b** concentrating on elements with a low expansion coefficients [16], reported by [16], except Ni data which were taken from [7].

in CTE is the result of the lower values of CTE for Cr, Re and Mo relative to that of Ni, offset by the atomic volume contributions of Cr, Re and Mo relative to Ni which has the effect of increasing CTE. The simple rule of mixtures approach in Eq. (5), however, becomes more complicated when predicting the CTE of a multi-phase alloy, as $\bar{\alpha}_i$ and V_i are likely to be different for each phase.

Empirical models

These models have been developed by fitting polynomials to a set of experimentally measured CTE values using regression analysis. The effects of Cr, Fe, Mo, W, (Nb + Ta), Mn, Si, Ti and Al on CTE of Ni–20Cr wt% alloys were modelled by Hull et al. [9] using a linear form up to 1000° F (538 °C)

$$\mathrm{CTE} = \beta_0 + \beta_1 C_1 + \beta_2 C_1^2 + \beta_3 C_2 + \beta_4 C_2^2 + \beta_5 C_1 C_2 + \beta_6 C_3 + \ldots, \quad (6)$$

where β_i are the regression coefficients and C_i are concentrations of alloying elements i. The contributions of second order terms were either too small (or not considered) except in the case of Cr, which has shown a maximum at around 23.6 wt% through the C_{Cr}^2 interaction. The above model has been validated against a number of commercial alloys.

For Ni-based alloys containing Cr, W, Mo, Al and Ti, Yamamoto et al. [13] derived the following formulation for the CTE of Fe-free Ni alloys from room to 700 °C:

$$\mathrm{CTE} = \left\{13.9 + 0.073\,C_{\mathrm{Cr}} - 0.08\,C_{\mathrm{W}} - 0.082\,C_{\mathrm{Mo}} - 0.018\,C_{\mathrm{Al}} - 0.16\,C_{\mathrm{Ti}}\right\} \times 10^{-6}, \quad (7)$$

where element concentrations are given in wt%. The results of work by Dosovitskiy et al. [14] on elements Cr and W to 800 °C using a series of Ni-W, Ni-Cr, and Ni-Cr-W alloys are shown by the following derivation:

$$\mathrm{CTE} = \{15.63 - (0.416C_{\mathrm{W}}) - 0.0097C_{\mathrm{Cr}}\} \times 10^{-6}, \quad (8)$$

where concentrations are given in at.%. Sung and Poirier [7] have derived a temperature- and concentration-dependent empirical CTE model for Ni-based superalloys comprising γ and γ' phase mixtures by fitting experimental data determined up to 1300 K (1027 °C) to the following form of linear relationship using regression

$$\mathrm{CTE} = d_0 + d_1 C_{\mathrm{Ti}} + d_2 C_{(\mathrm{Al+V})} + d_3 C_{\mathrm{Cr}} + d_4 C_{(\mathrm{Ta+Nb+Mo+W})}, \quad (9)$$

where C_i are the concentrations of element i in wt% and d_j, $j = 0\ldots3$ are fitting parameters which are functions of temperature. The concentrations of Al and V are summed together and coupled via a single d_2 parameter because their contribution to CTE was discovered to be similar. For the same reasons, the concentrations of Ta, Nb, Mo and W are added and included in Eq. (9) through d_4. The sum of concentrations of Ni and Co is considered as a dependent variable. The d_0 term is akin to the behaviour of CTE in Ni given by Eq. (3) as

$$d_0 = (b_0 + b_1 T^n + b_2 T^{2n} + b_3 T^{3n}) \times 10^{-5}, \quad (10)$$

where T is temperature in K, b_i, $i = 1\ldots3$ are fitting coefficients and n is 1 / 3 as for Ni in Eq. (3). The b_i up to 1300 K are given as $b_0 = -5.9431$, $b_1 = 2.5805$, $b_2 = -0.30383$ and $b_3 = 1.2181 \times 10^{-2}$. However, since extrapolation beyond 1300 K with these b_i gives rise to too much deviation from the CTE of γ-Ni given in Eq. (3), the following set of b_i has been derived for $T \geq 1300$ K by the authors: $b_0 = 6.9411 \times 10^{-2}$, $b_1 = 0.50692$, $b_2 = -6.5013 \times 10^{-2}$ and $b_3 = 3.0825 \times 10^{-3}$. The derivation is based on the observation made by Morrow et al. [10] that Ni-based superalloys containing γ and γ' have a smaller CTE compared to a single phase γ. When γ and γ' alloys are heated and transform to γ entirely, the CTE increases by an increment that depends on the fraction of γ'. Morrow et al. [10] quantified the increase of CTE for alloys containing Al and Mo as 0.6×10^{-6} $^{\circ}C^{-1}$.

Sung and Poirier [7] have also determined the temperature dependence of d_i ($i > 0$) by fitting experimental data at 400, 700, 1000 and 1100 K to the following equation, and the fitted coefficients p_i and q_i are shown in Table 1.

$$d_i = (p_i + q_i T) \times 10^{-5}. \tag{11}$$

Amongst the empirical models, the scheme of Sung and Poirier [7] encompasses the widest range of components, compositions and temperatures applicable for Ni-based superalloys. However, their model is derived for superalloy compositions, consisting mainly of γ/γ' mixtures and hence care has to be taken when the scheme is extended to bond coat compositions which normally contain the phase β and sometimes other phases such as α-Cr in high fractions.

Mixtures of phases

The CTE of an alloy can also be modelled by taking contributions of the thermal expansions of individual phases into account. A simple rule of mixtures approach can then be given by

$$\bar{\alpha} = \sum \bar{\alpha}_i V_i \,, \tag{12}$$

where $\bar{\alpha}$ is the CTE of the multi-phase body, $\bar{\alpha_i}$ are the CTEs of individual phases i, and V_i are the volume fraction of phases i. The method can be used to recognise the micro-stresses, termed tessellated stresses, which are known to develop between differentially expanding phases. The most recognised formula which accounts for the elastic stresses is given by the Turner's equation [25, 26]

$$\bar{\alpha} = \frac{\sum \bar{\alpha}_i V_i K_i}{\sum V_i K_i}, \tag{13}$$

where the additional K_i term represents the bulk modulus of phases i. The formula assumes only uniform hydrostatic stresses to exist within the phases. If the Poisson's ratios of the phases are identical, Young's moduli E_i can replace bulk moduli K_i in Eq. (13) which gives

$$\bar{\alpha} = \frac{\sum \bar{\alpha}_i V_i E_i}{\sum V_i E_i}. \tag{14}$$

In general, Turner's equation yields lower CTE values compared to the simple rule of mixtures method because the phases with low expansion coefficients are likely to have high elastic moduli [26].

Hermosilla et al. [27] calculate the CTE of a phase aggregate using a modified version of an expression derived by Wakashima et al. [28] given by

$$\bar{\alpha} = \frac{\sum V_i\{K_i/(K_i + \psi K)\}\bar{\alpha}_i}{\sum V_i\{K_i/(K_i + \psi K)\}}, \tag{15}$$

where $\bar{\alpha}_i$ are CTEs of individual phases and term ψ given as

$$\psi = \frac{2 - 4v}{1 + v}, \tag{16}$$

where v is the Poisson's ratio of the aggregate. For an isotropic phase aggregate, the elastic properties are defined by the bulk K and shear moduli G which can be calculated using bulk K_i and the shear G_i moduli of constituent phases i following the expressions originally derived by Budiansky [29], which are in turn based on Eshelby's inclusion technique [30, 31].

$$\sum \frac{V_i}{1 + \phi\{G_i/G - 1\}} = 1 \tag{17}$$

$$\sum \frac{V_i}{1 + \varphi\{K_i/K - 1\}} = 1 \,, \tag{18}$$

where ϕ and φ are defined by following expressions:

$$\phi = \frac{2(4 - 5v)}{15(1 - v)} \tag{19}$$

$$\varphi = \frac{(1 + 5v)}{3(1 - v)}. \tag{20}$$

Using the following standard relationship available for isotropic properties of phases

Table 1 Regression coefficients for Eq. (11).

i	p_i	q_i
1	-3.243×10^{-3}	-6.825×10^{-6}
2	-1.3×10^{-2}	1.469×10^{-5}
3	-1.567×10^{-2}	1.070×10^{-5}
4	-4.538×10^{-3}	-9.485×10^{-6}

$$v = \frac{3K - 2G}{6K + 2G}, \tag{21}$$

equations (15)–(21) can be used to calculate the CTE of the phase aggregate using a numerical root finding scheme for solving a non-linear systems of equations (e.g.[32]).

Although the phase mixture approaches are powerful, they have not been used widely in the past due to the difficulties in accurately determining phase volume fractions and elastic properties at high temperatures. Fortunately, due to the advancements in thermodynamic equilibrium calculation software such as MTDATA [33] and the wide availability of assessed thermodynamic parameter databases such as Ni DATA for Ni-based alloys [34], the task of determining phase fractions as a function of temperature and composition has now become possible for Ni-based superalloys and coatings (e.g. [35, 36]).

However, for the use of methods by Turner [25] and Hermosilla et al. [27], calculation of elastic properties of phases as a function of composition and temperature remains a problem for Ni-based alloys, and especially coatings, as a result of general lack of high-temperature data and suitable models.

Modelling strategy

In this work, the capability of the model introduced by Hermosilla et al. [27] ("Mixtures of phases" section) has been further developed to include temperature-dependent elasticity, density and phase composition data to calculate the CTE of a number of Ni-based superalloys and bond coats. The model predictions have then been compared with experimental data, both new data determined during the course of this work and those available in literature. The model predictions have also been compared with two other modelling schemes, a simple rule of mixtures method and Turner's scheme [25] ("Mixtures of phases" section), both of which take into account the phase constitution of the materials. The simple rule of mixtures method adopted here is illustrated in Fig. 3. The phase constitution of the material was calculated using thermodynamic equilibrium calculation software ("Determination of phase constitution" section) which returned the equilibrium weight fractions of phases for a given combination of chemical composition, temperature and pressure. The weight fraction ω_i of each phase i predicted to be present at the temperature was used to calculate the volume fraction of each phase present using the densities of each phase ρ_i. The volume-weighted CTE values of individual phases $\bar{\alpha}_i$ were combined using a simple rule of mixtures method given in Eq. (22) to obtain a value for the CTE of the material.

$$\bar{\alpha} = \frac{\sum \bar{\alpha}_i \{\omega_i/\rho_i\}}{\sum \{\omega_i/\rho_i\}}. \tag{22}$$

Determination of phase constitution

The equilibrium phase structure as a function of material composition, temperature and pressure was calculated using the Version 5.02 of the Application Program Interface (API) of MTDATA software (Linux Version) [33] together with the Ni-DATA thermodynamic parameter database Version 3.1 [34].

Modelling of the bulk modulus of phases

For the implementation of the methods of Turner [25] and Hermosilla et al. [27], the elastic properties of the constituent phases of the material are needed. Systematically derived elastic properties of multi-component alloy phases are unavailable, and hence, data for pure materials are used in this work. The values for bulk modulus (K) of γ-Ni up to 762 K have been derived in [37] using experimental data determined by Alers et al. [38], and these have been adopted here by fitting a third-degree polynomial of the following form:

$$K_i = a_0 + a_1 T + a_2 T^2 + a_3 T^3, \tag{23}$$

where K_i are given in GPa and T in K. The fitted polynomial coefficients a_i are given in Table 2 which also shows the coefficients obtained in a similar manner for γ' up to 1100 K derived from work of Tanaka and Koiwa [39] and for β up to 875 K by Rusović and Warlimont [40].

For higher temperatures, isentropic bulk moduli calculated using a first-principles approach by Wang et al. [37]

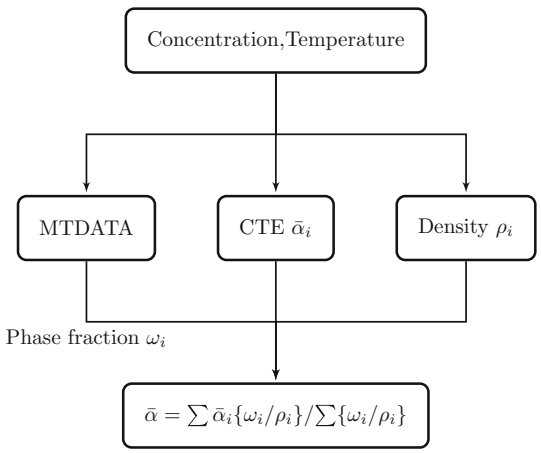

Fig. 3 A schematic illustration of the simple rule of mixtures method used to calculate the CTE as a function of material composition and temperature.

were used, after fitting the third-degree polynomial given in Eq. (23). The fitted polynomial coefficients are given in Table 2.

For the γ and γ' phases, data calculated without the quasistatic approximation were used, whereas for the β phase, those obtained with the quasistatic approximation were used, as these sets showed best correspondence with lower temperature experimental data in [38–40]. Due to the unavailability of moduli data for the α-Cr and σ phases, the bulk modulus of 161 GPa reported for pure Cr at room temperature [41] was used for both of these phases as an approximation, due to the high amount of Cr likely to be present in these phases.

Modelling of Poisson's ratios of the phases

The Poisson's ratios of γ, γ' and β phases were calculated using modelled stiffness coefficients c_{11} and c_{12} in [37], which showed reasonable agreement with low-temperature experimental data, using the following relationship which holds for isotropic materials:

$$v = \frac{c_{12}}{c_{12} + c_{11}}. \tag{24}$$

The stiffness parameters as well as the Poisson's ratios v_i of phases i were modelled using a third-degree polynomial of the form given in Eq. (25), where temperature T is given in K. The coefficients of best fit are given in Table 3.

$$v_i = a_0 + a_1 T + a_2 T^2 + a_3 T^3. \tag{25}$$

The Poisson's ratios of α-Cr and σ phase have yet to be determined, and hence, the reported value of 0.21 for pure Cr at room temperature [41] was used for both of these phases here as an approximation.

Modelling of the density of phases

The density ρ_i of each phase i of the material was used to calculate the volume fraction v_i of the phase using the standard expression

$$v_i = \frac{w_i}{\rho_i \sum\{w_i/\rho_i\}}, \tag{26}$$

where w_i is the mass fraction of phase i returned from the thermodynamic calculations. The density ρ of the γ and γ' phases was determined using the standard expression for fcc crystals

$$\rho = \frac{4\sum M_j X_j}{N_0 a^3}, \tag{27}$$

where M_j and X_j are the atomic weight and fractional concentration of element j, N_0 is Avogadro's number and a is the lattice parameter of the alloy. The lattice parameter was modelled using the Vegard's Law [42]

$$a = a_0 + \sum_j^n X_j \frac{\partial a}{\partial X_j}, \tag{28}$$

where a_0 are 3.5219 and 3.5691 Å for γ and γ', respectively, and $\partial a/\partial X_j$ for various elements in γ and γ' were obtained from work by Kablov et al. [43] and are shown in Table 4.

The density ρ of a phase at temperature T was determined using the general relationship

$$\rho_i = \rho_0[1 + \alpha(T - T_0)]^{-3}, \tag{29}$$

where ρ_0 is the density of the phase at room temperature T_0 and α its CTE. In the absence of a model for calculating density as a function of composition in the γ phase, the reported ρ of pure Ni was used in Eq. (29).

The density of β-NiAl was given as a function of Ni concentration by Noebe et al. [23] using data from a number of sources. The density decreases linearly with decreasing Ni content, although a change in slope of the line occurs at the stoichiometric composition which has a density of 5.9 g cm^{-3}. Due to the discontinuity at the stoichiometric concentration, 50 at.% Al, two schemes are used to determine the density ρ_{NiAl} above and below this composition which are modelled as follows: for $40 < C_{Ni} < 50$ at.%

$$\rho_{NiAl} = 3.15 + 0.055\, C_{Ni} \tag{30}$$

and for $50.0 < C_{Ni} < 55.0$ at.%

Table 2 Parameters used for the polynomial expression for the bulk modulus K (GPa) in Eq. (23) for γ, γ' and β phases.

Temperature	a_0	a_1	a_2	a_3	Ref
	γ-Ni				
<762 K	187.76342	-5.98×10^{-3}	-3.03682×10^{-5}	1.42354×10^{-8}	[38]
>762 K	192.03651	-1.738×10^{-2}	-1.2231×10^{-5}	1.17529×10^{-9}	[37]
	γ'-Ni_3Al				
<1100 K	183.46354	-3.876×10^{-2}	2.87653×10^{-5}	-2.00323×10^{-8}	[39]
>1100 K	174.31833	-7.77×10^{-3}	-1.90219×10^{-5}	5.32998×10^{-9}	[37]
	β-NiAl				
<875 K	161.65147	-1.922×10^{-2}	5.48313×10^{-6}	-3.86176×10^{-9}	[39]
>875 K	153.93791	-6.08×10^{-3}	-6.46951×10^{-6}	3.1233×10^{-10}	[37]

Table 3 Parameters extracted for the polynomial expansion of the Poisson's ratios (ν) in Eq. (23) for various phases.

Phase i	a_0	a_1	a_2	a_3
γ-Ni	3.6485×10^{-1}	-2.3397×10^{-6}	2.1377×10^{-9}	-1.2033×10^{-12}
γ'-Ni_3Al	3.8090×10^{-1}	4.9669×10^{-6}	-9.4745×10^{-9}	3.5822×10^{-12}
β-NiAl	3.9071×10^{-1}	2.7860×10^{-6}	4.6282×10^{-9}	-4.7916×10^{-13}

Table 4 The rate of increase of lattice parameter in the γ and γ' phases, with fractional increment of atomic concentration of alloying elements.

	$\partial a/\partial X_j$ (Å)	
Element j	γ	γ'
Al	0.221	–
Co	0.059	−0.002
Cr	0.122	0.014
Hf	1.559	1.339
Mo	0.412	0.097
Nb	0.595	0.275
Re	0.382	−0.50
Ru	0.303	0.083
Ta	0.693	0.398
Ti	0.302	0.149
V	0.142	−0.189
W	0.435	0.151

$$\rho_{\mathrm{NiAl}} = 0.118\, C_{\mathrm{Ni}}. \tag{31}$$

Implementation of the models

The models were coded using the C language with the MTDATA software library being linked via its Application Program Interface (API) [44]. In order to solve the non-linear system given in Eqs. (15)–(21) for the scheme of Hermosilla et al. [27], a C routine based on that given in [32] for the multidimensional downhill-simplex method of Nelder and Mead [45] was used.

Experimental method

In order to provide additional validation, the thermal expansion in an IN-738LC superalloy and Amdry-995 bond coat material was measured in a Linseis mechanical dilatometer equipped with an alumina test piece holder and push-rod. The nominal chemical compositions of the samples are given in Table 5. The instrument was calibrated in accordance with ASTM E228/CEN EN821-1. The transducer sensitivity was determined using a calibrated drum micrometer, and the instrument baseline shift was determined using a piece of push-rod alumina as a test piece. The apparatus expansion correction was determined using a platinum test piece and reference data for platinum taken from [46]. For each test piece, at least three thermal cycles were employed at a heating/cooling rate of 2° min^{-1} using a flushed argon atmosphere to restrict oxidation. The first thermal cycle was used for settling and annealing of the test piece, and the thermal expansion data were taken from second and third cycles as the average of heating and cooling. The accuracy of the determined expansion coefficients is considered to be about $\pm 0.1 \times 10^{-6}$ $^\circ\mathrm{C}^{-1}$ for temperature ranges from room to above 400 °C.

The measurements were carried out in IN-738LC samples cut in the shape of a bar with approximate dimensions $28 \times 8 \times 3$ mm^3 to 1200 °C. A delaminated layer of sample was used in the case of Amdry-995 and reliable measurements could be collected only up to 800 °C due to the fragility of the sample.

Results and discussion

The graphs in Figs. 4a–c show a comparison between the measured and calculated CTEs of superalloys IN-738LC and CMSX-4 and also for the bond coat Amdry-995. The experimental measurements of CTEs in the IN-738LC and Amdry-995 samples were made during the current study, and those in CMSX-4 were extracted from the study in [47]. The nominal compositions of the materials are listed in Table 5, which were used as input for the modelling (except Y which was not supported by the thermodynamic database). The calculated CTE profiles shown in the Fig. 4 have been produced using three schemes: (1) that proposed by Hermosilla et al. [27] which has been extended in this work with the incorporation of temperature-dependent elastic, density and phase composition data, (2) Turner's method [25] described in "Mixtures of phases" section using temperature-dependent elastic, density and phase composition data and (3) the simple rule of mixtures (ROM) method described in "Modelling strategy" section with temperature-dependent density and phase composition data.

As the graphs reveal, the model predictions are in very good agreement with experiment measurements. At higher temperatures, above 950 °C in IN-738LC and above 850 °C in CMSX-4, the model starts to underpredict the CTE slightly. In Amdry-995, again an excellent match could be found within the temperature range 400–800 °C but above 650 °C, the calculations over-predicts the measured CTE by a small margin.

The discrepancies seen between experimental and modelled profiles can be related to the phase structure

Table 5 Nominal compositions of the substrate and coating materials.

Alloy	Concentration (wt%)									
	Al	Co	Cr	Mo	Nb	Re	Ta	Ti	W	Y
IN-738LC	3.40	8.50	16.0	1.75	0.90	–	1.75	3.40	2.60	–
CMSX-4	5.6	9.00	6.50	0.60	–	3.00	6.50	1.00	6.40	–
Amdry-995	8.00	38.50	21.00	–	–	–	–	–	–	0.5

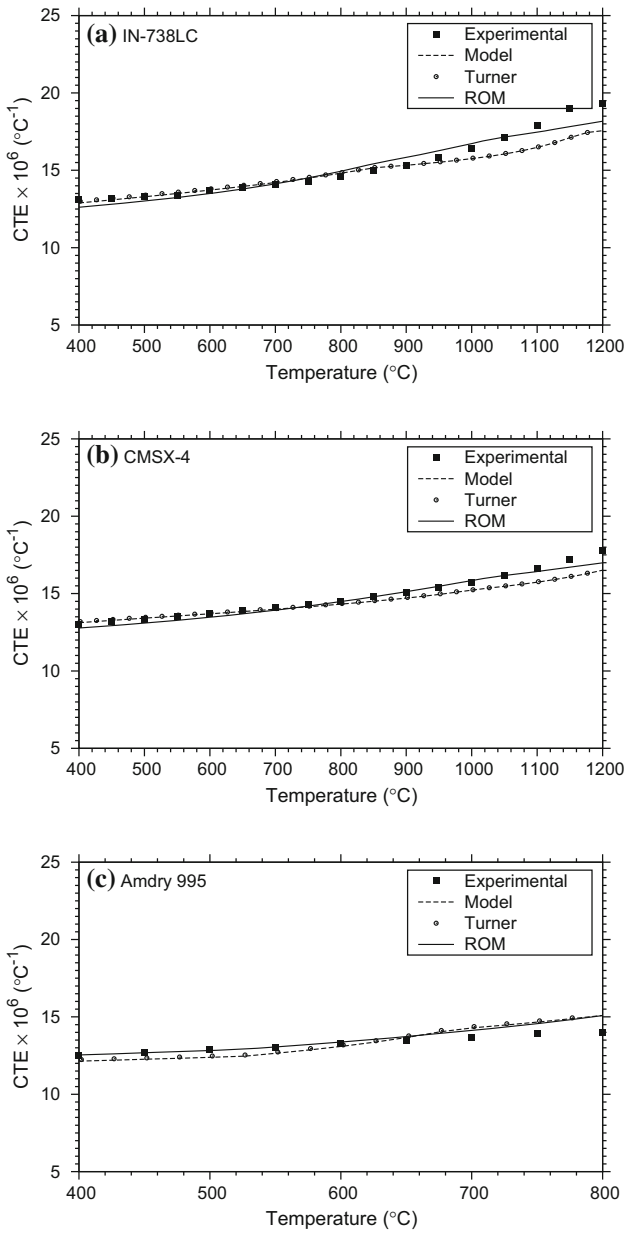

Fig. 4 Comparison between experimentally determined CTE values of **a** IN-738LC, **b** CMSX-4 and **c** Amdry-995, and predictions by a number of models which use phase constitution into account. Model refers to the extended model originally proposed by Hermosilla et al. [27]. Turner and ROM refer to the models by Turner [25] and the simple rule of mixtures method described in "Modelling strategy" section and Fig. 3, respectively.

variation between samples. Figure 5 shows the predicted phase structure variation with temperature for each sample calculated in this work. For the superalloy substrates IN-738LC and CMSX-4, the phase structure at lower temperatures consists of γ, γ' and σ phases. As temperature is increased, first the σ and then γ' is dissolved from the structure, and the temperature at which the predicted CTEs start to deviate from measured values coincides with the disappearance of the σ phase. Therefore, the modest disagreement observed between the experimental and modelled curves at higher temperatures in Fig. 4a, b could be due to a delay in dissolution of the σ phase in particular or due to an underestimation of the CTE values of γ and γ' phases at higher temperatures. The model however is still capable of estimating the CTE with a high degree of accuracy in the temperature range where these materials are commonly used in practice.

In the case of the Amdry-995 bond coat sample, the phase structure is predicted to contain also the β phase in addition to γ, γ' and σ phases, as Fig. 5c reveals. Above 500 °C, the amount of σ and γ' gradually decreases while the γ and β content does the opposite, although beyond 700 °C, the β concentration declines. Despite the complexity in the phase transitions, the model predicts the CTE of this sample reasonably accurately as evident in Fig. 4c, with only a slight deviation occurring at around 620 °C which overlaps with the substantial phase structure change observed in Fig. 5c.

The CTE calculation scheme of [27] requires the determination of elastic properties of the specimen material using the properties of its constituent phases, as outlined in Eqs. (17)–(21). The model developed to calculate the elastic properties of individual phases for this purpose is described in "Modelling of the bulk modulus of phases and Modelling of Poisson's ratios of the phases" sections. The bulk moduli of individual phases calculated using this model are shown in Fig. 6a–c as a function of temperature, along with the bulk moduli of superalloys IN-738LC, CMSX-4 and bond coat Amdry-995 obtained via Eqs. (17)–(21). According to the figure, the bulk moduli K_i of individual phases i vary according to $K_\beta > K_{\gamma'} > K_\gamma > K_\sigma$, and therefore, it is reasonable to assume that the modulus of a superalloy, which consists mainly of the γ and γ' phases, should generally lie between

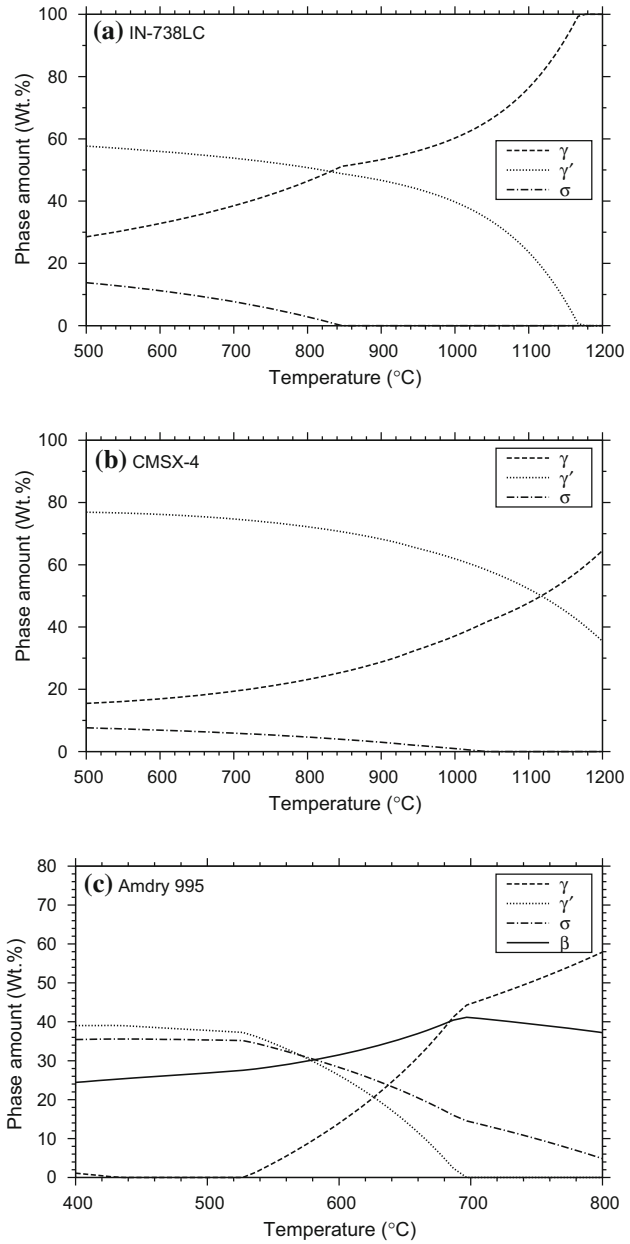

Fig. 5 Predicted phase composition variation with temperature of superalloys **a** IN-738LC and **b** CMSX-4, and **c** MCrAlY bond coat Amdry-995.

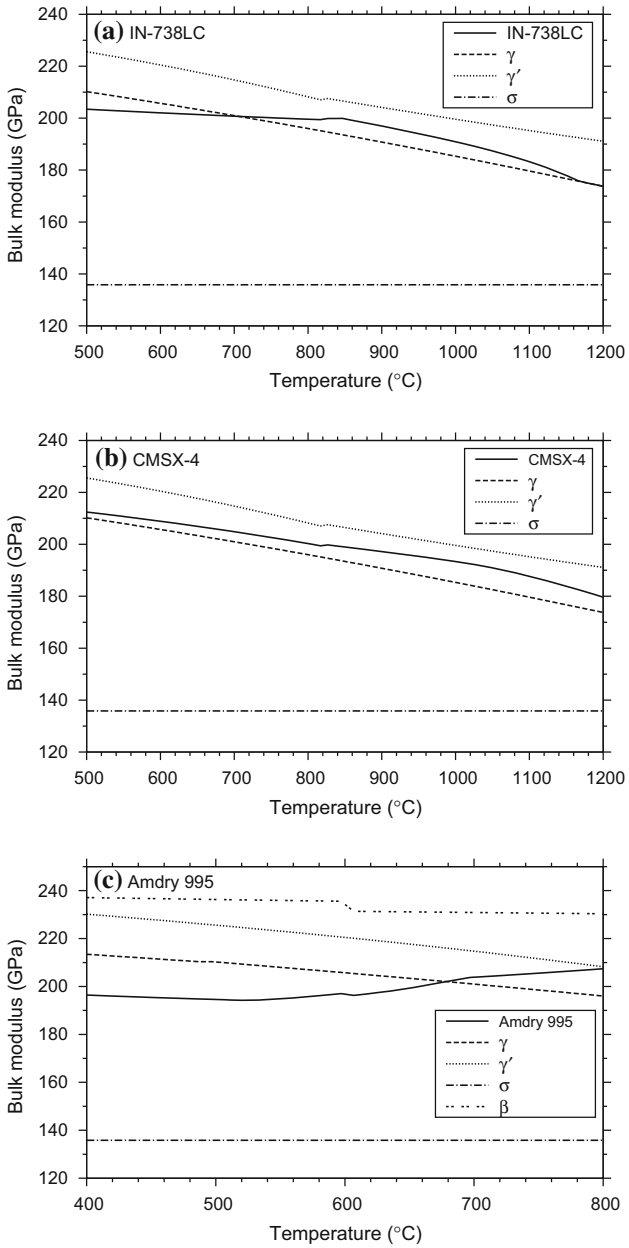

Fig. 6 Calculated variation of bulk modulus with temperature of **a** IN-738LC, **b** CMSX-4 and **c** Amdry-995 specimens and their constituent phases.

the moduli of those two phases, as evident indeed in the case of CMSX-4. However, the presence of a fairly high fraction of α, σ or other TCP phases at lower temperatures, such as in IN-738LC, can cause the modulus to be lower than that of γ at low temperatures. It is noted here that due to the lack of data, the temperature variation of the σ and α is assumed to be constant in the current model. In Amdry-995 and other such coating compositions, the high proportion of the β phase present, which can be stable up to high temperatures, can increase the modulus of the coating over that of a superalloy composition, as illustrated in Fig. 6.

Figure 7 shows the variation of calculated shear modulus of γ, γ' and β phases using the model given in "Modelling of the bulk modulus of phases and Modelling of Poisson's ratios of the phases" sections and also that of Amdry-995 computed using the moduli of phases via Eqs. (17)–(21). As shown, the shear modulus G_i of phases i shows the relationship $G_\sigma > G_\gamma > G_{\gamma'} > G_\beta$. At temperatures lower than 650 °C, the shear modulus of Amdry-995

is higher than that of γ as the phase structure has a high proportion of σ phase which is shown to have a high shear modulus. As temperature is increased, the shear modulus of Amdry-995 goes lower than that of γ because of the dominance of the γ and β phases at these temperatures which have lower moduli compared to the σ phase.

The overall agreement shown in Fig. 4 between experimental measurement and predictions by a number of models is very good. All three models account for the phase constitution of the materials but the schemes provided by Hermosilla et al. [27] and Turner [25] additionally consider the elastic properties of constituent phases.

At above 850 °C in the case of superalloys and IN-738LC in particular, the model predictions deviate from measured values. The method of simple rule of mixtures gives much better predictions, up to 1100 °C, than the models which incorporates elastic properties of phases, which tend to underpredict the CTEs at higher end of the temperature scale. It could be possible that at high temperatures, the modelled elastic properties are less accurate and further work is needed to develop that part of the model.

It should also be mentioned that during experimental measurement at a typical heating/cooling rate, the equilibrium amounts of phases are never present, possibly more during heating and less during cooling from above the solvus. There is often hysteresis in thermal expansion curves in the apparent solvus temperature range. These artefacts may well have affected the agreement between model predictions and experimental data observed.

Interestingly, both methods that incorporate elastic properties of phases give very similar predictions for the examined alloy compositions over the temperature range considered. While the approach by Hermosilla et al. [27] provides a rigorous method of taking account of interactions between phases, in practice, almost exactly the same results have been achieved for the specific materials considered here using simpler methods which do not need so much data. The main purpose of the method by Hermosilla et al. [27] is therefore to provide a rigorous validation of what are effectively semi-empirical phase mixture models which might or not apply to other multi-phase alloys.

The graph in Fig. 8 shows how the predicted CTE values of a number of Ni-based superalloys and coatings compare with the measured CTE figures available in literature at 1000 K (726.85 °C). There is in general a good agreement between experiment and modelling with many points overlying on the dashed line which represents exact one to one correspondence. The calculated root mean square value of the difference between the model and measurement figures of all the points shown in Fig. 8 is 0.6103×10^{-6} °C^{-1}, indicating that the model can predict the CTE with a high degree of accuracy in this case.

It should be mentioned, however, that the CTE of a material can also be affected by factors such as grain size, homogeneity and crystalline texture which the current model does not take into account. Furthermore, the thermodynamic modelling procedure used in this work has limitations, for example, some elements and phases may not be supported. Although the predictions are very good as discussed, some of these factors may have contributed to the discrepancies observed in Figs. 4 and 8.

Conclusions

Most of the models currently available for predicting CTEs of nickel-based superalloys are empirical in nature and therefore are restricted by the temperature or the

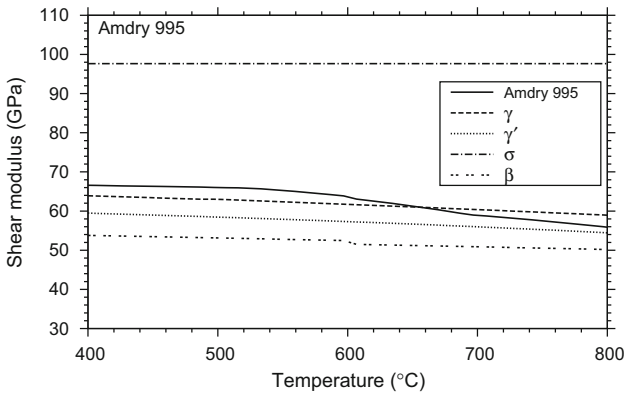

Fig. 7 Calculated variation of shear modulus with temperature of Amdry-995 specimens and its constituent phases.

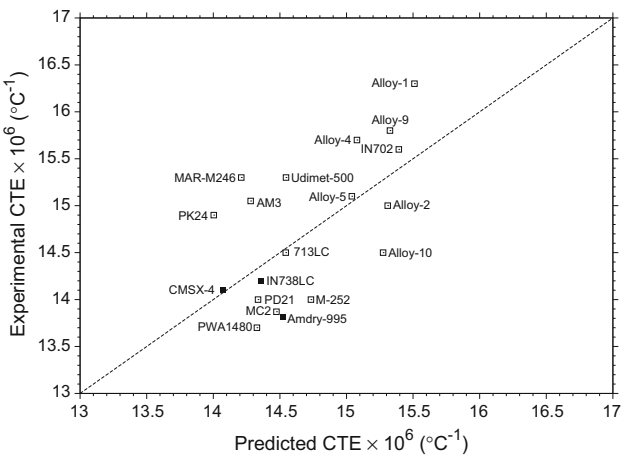

Fig. 8 Comparison between experimentally measured CTE values and those predicted using the model described in [27] that has been extended in this work. The values shown are for 1000 K (726.85 °C) for a number of superalloys. The experimental data are mainly from [7] (*open markers*).

composition range in which the experiments were carried out. Models based on foundations of materials physics are very limited. The recent advances in modelling thermodynamic properties based on CALPHAD techniques and the availability of reliable assessed databases for Ni-based alloys make it possible to predict phase constitution of such alloys accurately. As material properties such as CTE are very likely to be dependent on the phase structure and the CTEs of individual phases in an alloy, it is possible to exploit advances made in such thermodynamic modelling to develop better CTE prediction models. In this work, a model originally proposed by Hermosilla et al. [27] has been further developed to incorporate temperature-dependent elasticity, density and phase composition data, and the CTE predictions by the extended model have been compared against measured CTEs of superalloys IN-738LC, CMSX-4 and bond coat Amdry-995. The predictions agree very well at lower temperatures, but the model slightly under-predicts the CTE in the superalloys considered at higher temperatures. For the Amdry-995, IN-738LC and CMSX-4 compositions examined, the method of [27] gave close results to those predicted by the model proposed by Turner [25]. As both methods are based on the same elastic properties and phase prediction models, comparable results can be expected. The work also found that simple volume-weighted rule of mixtures method, which does not take elastic properties into consideration, can also predict experimental measurements of CTEs appreciably well, and even give better agreement at high temperatures. It has also been identified that further work is still needed to improve the elastic parameter models.

Acknowledgements We would like to acknowledge the support of The Energy Programme, which is a Research Councils UK cross council initiative led by EPSRC and contributed to by ESRC, NERC, BBSRC and STFC, and specifically the Supergen initiative (Grants GR/S86334/01 and EP/F029748) and the following companies: Alstom Power Ltd., Doosan Babcock, E.ON, National Physical Laboratory, Praxair Surface Technologies Ltd, QinetiQ, Rolls-Royce plc, RWE npower, Siemens Industrial Turbomachinery Ltd. and Tata Steel, for their valuable contributions to the project.

Compliance with ethical standards

Conflict of Interest The authors declare that they have no conflict of interest.

References

1. Sims CT, Stoloff NS, Hagel WC (1987) Superalloys II: high-temperature materials for aerospace and industrial power. Wiley, New York
2. Reed RC (2006) The superalloys: fundamentals and applications. Cambridge University Press, Cambridge
3. Jena AK, Chaturvedi MC (1984) The role of alloying elements in the design of nickel-base superalloys. J Mater Sci 19(10):3121–3139. doi:10.1007/BF00549796
4. Tawancy HM, Sridhar N, Abbas NM, Rickerby DS (2000) Comparative performance of selected bond coats in advanced thermal barrier coating systems. J Mater Sci 35(14):3615–3629. doi:10.1023/A:1004825932601
5. Evans HE, Taylor MP (1997) Creep relaxation and the spallation of oxide layers. Surf Coat Technol 94–95(1–3):27–33
6. Liang JJ, Wei H, Zhu YL, Sun XF, Hu ZQ, Dargusch MS, Yao X (2011) Phase constituents and thermal expansion behavior of a NiCrAlYRe coating alloy. J Mater Sci 46(2):500–508. doi:10.1007/s10853-010-4953-y
7. Sung PK, Poirier DR (1998) Estimation of densities and coefficients of thermal expansion of solid Ni-base superalloys. Mater Sci Eng A 245(1):135–141
8. Giamei AF, Pearson DD, Anton DL (1985) γ: The key to superalloy behaviour. In: Koch CC, Liu CT, Stoloff NS (eds) High-temperature ordered intermetallic alloys. Materials Research Society Symposia Proceedings, vol. 39, p 294–308. Materials Research Society, Pittsburgh
9. Hull FC, Hwang SK, Wells JM, Jaffee RI (1987) Effect of composition on thermal expansion of alloys used in power generation. J Mater Eng 9(1):81–92
10. Morrow H, Sponseller DL, Semchyshen M (1975) The effects of molybdenum and aluminum on the thermal expansion coefficients of nickel-base alloys. Metall Mater Trans A 6(3):477–485
11. Pavlovic AS, Babu VS, Seehra MS (1996) High-temperature thermal expansion of binary alloys of Ni with Cr, Mo and Re: a comparison with molecular dynamics simulations. J Phys 8(18):3139–3149
12. Mei J, Cooper BR, Hao YG, Vanscoy FL (1994) Molecular dynamics modeling using abinitio interatomic potentials for thermal properties of ni-rich alloys. In: Stocks GM, Turchi PEA (eds) Alloy modeling and design. Symposium on alloy modeling and design, held during the 1993 Materials Week of the Minerals-Metals-and-Materials-Society, Pittsburgh, 18–20 October, 1993, p 165–174
13. Yamamoto R, Kadoya Y, Kawajand H, Magoshj R, Noda T, Hamano S, SUeta, Isobe S (2002) New wrought Ni-based superalloys with low thermal expansion for 700°C steam turbines. In: Lecomte-Beckers J, Carton M, Schubert F, PJ Ennis (eds) Materials for advanced power engineering 2002. Proceedings of the seventh Liège conference on energy and technology, vol. 21, p 1351–1360. Forschungszentrum Jülich GmbH and Institut für Werkstoffe und Verfahren der Energietechnik, September 30–October 3
14. Dosovitskiy GA, Samoilenkov SV, Kaul AR, Rodionov DP (2009) Thermal expansion of Ni-W, Ni-Cr, and Ni-Cr-W alloys between room temperature and 800°C. Int J Thermophys 30(6):1931–1937
15. Kim DE, Shang SL, Liu ZK (2012) Effects of alloying elements on thermal expansions of γ-Ni and γ'-Ni_3Al by first-principles calculations. Acta Metall 60(4):1846–1856
16. Touloukian YS (1970) Thermal expansion, metallic elements and alloys. Thermophysical properties of matter: the TPRC data series; a comprehensive compilation of data, vol. 12. IFI/Plenum, New York

17. Arbuzov MP, Zelenkov IA (1964) Thermal expansion of certain transition metals and alloys on their base. Fiz Met Metalloved 18(2):311–312
18. Taylor A, Floyd RW (1952-1953) The constitution of nickel-rich alloys of the nickel-titanium-aluminium system. J Inst Met 81:25
19. Williams RK, Graves RS, Weaver FJ, McElroy DL (1984) Physical properties of Ni_3Al containing 24 and 25 atomic percent aluminum. In: High-temperature ordered intermetallic alloys I. MRS Proceedings, vol. 39, p 505–512. Materials Research Society, 1984. Symposium G
20. Ramesh R, Pathiraj B, Kolster BH (1992) Thermal evidence for the structural instability in Ni_3Al alloys. Mater Sci Eng A 152(1—-2):60–66 Proceedings of the Second International ASM Conference on High Temperature Aluminides and Intermetallics
21. Mohan Rao PV, Satyanarayana Murthy K, Suryanarayana SV (1993) High temperature thermal expansion characteristics of Ni_3Al alloys. J Alloys Compd 190:L33–L35
22. Porter WD, Maziasz PJ (1993) Thermal expansion data on several iron- and nickel-aluminide alloys. Scr Metall Mater 29(8):1043–1048
23. Noebe RD, Bowman RR, Nathal MV (1993) Physical and mechanical properties of the B2 compound NiAl. Int Mater Rev 38(4):193–232
24. Fritscher K, Leyens C, Peters M (1995) Development of a low-expansion bond coating for Ni-base superalloys. Mater Sci Eng A 190(1–2):253–258
25. Turner PS (1946) Thermal-expansion stresses in reinforced plastics. J Res Natl Bur Stand 37(4):239–250 Research Paper RP1745. U. S, Department of Commerce
26. Fahmy AA, Ragai AN (1970) Thermal-expansion behavior of two-phase solids. J Appl Phys 41:5108–5111 Symposium on thermal expansion of solids/composites, carbides
27. Hermosilla U, Karunaratne MSA, Jones IA, Hyde TH, Thomson RC (2009) Modelling the high temperature behaviour of TBCs using sequentially coupled microstructural-mechanical FE analyses. Mater Sci Eng A 513–514:302–310
28. Wakashima K, Otsuka M, Umekawa S (1974) Thermal expansions of heterogeneous solids containing aligned ellipsoidal inclusions. J Compos Mater 8(10):391–404
29. Budiansky B (1965) On the elastic moduli of some heterogeneous materials. J Mech Phys Solids 13(4):223–227
30. Eshelby JD (1951) The force on an elastic singularity. Philos Trans R Soc Lond Ser A 244:87–112
31. Eshelby JD (1957) The determination of the elastic field of an ellipsoidal inclusion, and related problems. Proc R Soc Lond Ser A 241(1226):376–396
32. Press William H, Teukolsky Saul A, Vetterling William T, Flannery Brian P (1992) Numerical recipes in C: the art of scientific computing, 2nd edn. Cambridge University Press, Cambridge
33. Davies RH, Dinsdale AT, Gisby JA, Robinson JAJ, Martin SM (2002) MTDATA-thermodynamics and phase equilibrium software from the National Physical Laboratory. CALPHAD 26(2):229–271
34. Saunders N (1996) Phase diagram calculations for Ni-based superalloys. In: Kissinger RD, Nathal MV, Deye DJ, Pollock TM, Anton DL, Woodford DA, Cetel AD (eds) Proceedings of the eighth international symposium on superalloys (superalloys 1996), p 101–110, Seven Springs. The Minerals, Metals & Materials Society
35. Karunaratne MSA, Ogden SL, Kenny SD, Thomson RC (2009) A multicomponent diffusion model for prediction of microstructural evolution in coated Ni-based superalloy systems. Mater Sci Technol 25(2):287–299
36. Karunaratne MSA, Di Martino I, Ogden SL, Oates DL, Thomson RC (2011) Modeling of microstructural evolution in an MCrAlY overlay coating on different superalloy substrates. Metall Mater Trans A 43(2):774–788
37. Wang Y, Wang JJ, Zhang H, Manga VR, Shang SL, Chen LQ, Liu ZK (2010) A first-principles approach to finite temperature elastic constants. J Phys 22:1–8 Article Number: 225404
38. Alers GA, Neighbours JR, Sato H (1960) Temperature dependent magnetic contributions to the high field elastic constants of nickel and an Fe-Ni alloy. J Phys Chem Solids 13(1–2):40–55
39. Tanaka K, Koiwa M (1996) Single-crystal elastic constants of intermetallic compounds. Intermetallics 4:S29–S39 Supplement 1
40. Rusović N, Warlimont H (1977) The elastic behaviour of β_2-NiAl alloys. Phys Status Solidi A 44(2):609–619
41. Lenkkeri JT, Lähteenkorva EE (1978) An investigation of elastic moduli of vanadium-chromium alloys. J Phys 8(8):1643–1651
42. Vegard L (1921) Die konstitution der mischkristalle und die raumfüllung der atome. Zeitschrift für Physik 5(1):17–26
43. Kablov EN, Petrushin NV, Bronfin MB, Alekseev AA (2006) Specific features of rhenium-alloyed single-crystal nickel superalloys. Russ Metall 2006(5):406–414
44. Davies RH, Dinsdale AT, Gisby JA (1998) MTDATA Handbook: Application Interface Programming Guide. National Physical Laboratory, Teddington
45. Nelder JA, Mead R (1965) A simplex-method for function minimization. Comput J 7(4):308–313
46. Hahn TA, Kirby RK (1972) Thermal expansion of platinum from 293 to 1900 K. In: Graham MG, Hagy HE (eds) Thermal expansion symposium 1971, vol 3., AIP conference proceedings, American Institute of Physics, New York, p 87–95
47. Quested PN, Brooks RF, Chapman L, Morrell R, Youssef Y, Mills KC (2009) Measurement and estimation of thermophysical properties of nickel based superalloys. Mater Sci Technol 25(2): 154–162